

# Anomalous protein adsorption/desorption kinetics on low-fouling surfaces

Mohammadhasan Hedayati,<sup>1</sup> Matt J. Kipper,<sup>1,2,3</sup> and Diego Krapf<sup>2,3,4</sup>

<sup>1</sup>*Department of Chemical and Biological Engineering,  
Colorado State University, Fort Collins, CO 80523, USA*

<sup>2</sup>*School of Biomedical Engineering, Colorado State University, Fort Collins, CO 80523, USA*

<sup>3</sup>*School of Advanced Materials Discovery, Colorado State University, Fort Collins, CO 80523, USA*

<sup>4</sup>*Department of Electrical and Computer Engineering,  
Colorado State University, Fort Collins, CO 80523, USA\**

In this work, protein-surface interactions were probed in terms of adsorption and desorption of a model protein, bovine serum albumin, on a low fouling surface with single-molecule localization microscopy. Single-molecule experiments enable precise determination of both adsorption and desorption rates. Strikingly the experimental data show anomalous kinetics, evident as a surface dwell time distribution that exhibits a power-law distribution, i.e. a heavy-tailed rather than the expected exponential distribution. As a direct consequence of this heavy-tailed distribution, the average desorption rate depends upon the time scale of the experiment and the protein surface concentration does not reach equilibrium. Further analysis reveals that the observed anomalous desorption emerges due to reversible formation of a small fraction of soluble protein multimers (small oligomers), such that each one desorbs from the surface with a different rate. The overall kinetics can be described by a series of elementary reactions, yielding simple scaling relations that predict experimental observations. This work reveals a mechanistic origin for anomalous adsorption/desorption kinetics that can be employed to interpret observations where low-protein fouling surfaces eventually foul when in long-term contact with protein solutions and provides new insights that can be used to define design principles for non-fouling surfaces and to predict their performance.

The interaction of proteins in solution with solid surfaces is a fundamental phenomenon of great importance in multiple scientific and engineering fields [1–5]. From a life sciences and biophysics perspective, adsorption and desorption of proteins at surfaces are key players in e.g. organ development, tissue repair, and blood clotting. In the biomedical implant and devices field, controlling or inhibiting irreversible protein adsorption has long been considered an important feature of biocompatible materials and biosensor surfaces [6–8]. When a biomedical device such as a catheter, or an implant such as a sent or artificial knee comes in contact with body fluids, they are exposed to a myriad of proteins apt to adsorbing into the foreign material and rapidly modifying the surface chemistry. This adsorbed protein layer can modulate subsequent biological phenomena including blood clotting, bacterial adhesion, and inflammation, which can lead, for example, to failure of blood-contacting medical devices, fouling of contact lenses, and deterioration of biosensor sensitivity. Many industrial technologies also rely on controlled protein adsorption for processes related to protein purification, drug delivery systems, food packaging and storage, and biosensing [1].

A key feature of irreversible adsorption onto solid surfaces involves surface-induced protein fouling. Thus, a great deal of effort has been placed in the design of advanced materials to impart protein resistance [9]. Besides their critical applications in biomaterials, low-fouling surfaces are routinely used in single-molecule biophysics research [10]. The most widely used and best characterized strategy to impart protein resistance to a surface consists of coating it with a polyethylene glycol (PEG) brush [11].

While many studies focus specifically on the rate of surface adsorption, the study of protein desorption from low-fouling surfaces is still lacking detailed understanding.

Adsorption and desorption processes are most often quantified in terms of the respective kinetic coefficients  $k_{\text{ads}}$  and  $k_{\text{des}}$  [7]. This analysis enables experiments to be interpreted using a basic kinetic equation

$$\frac{d\rho}{dt} = k_{\text{ads}} - \rho k_{\text{des}}, \quad (1)$$

where  $\rho$  is the adsorbed protein surface density and the adsorption coefficient is proportional to the bulk protein concentration. This simple kinetic model is expected to predict valid results for low surface occupancy so that the density of available surface sites and the protein solution concentration do not change substantially during protein adsorption. Eq. (1) is often sufficient to interpret short-term protein adsorption experiments and predicts that surface concentration will converge exponentially to a constant value ( $k_{\text{ads}}/k_{\text{des}}$ ) with a characteristic time constant  $1/k_{\text{des}}$ . However, it often fails to predict long-term (more than 30 min) surface kinetics. The failure of the kinetic equation (Eq. (1)) is sometimes ascribed to a deterioration of the non-fouling behavior due to various effects such as oxidation of the surface or the Vroman effect for complex protein mixtures [12].

In this letter, we study the kinetics of a generic globular protein, namely bovine serum albumin (BSA), on a PEG brush-coated surface. The kinetics are characterized in detail by employing single-molecule detection. Desorption from the surface is observed to exhibit anomalous behavior that is manifested as a power-law distribution

in the dwell times for particles on the surface. This behavior can be accurately explained by considering that there is a finite probability for the molecules in solution to reversibly self-associate. A simple model considering an equilibrium concentration of multimers in solution and a probability of dissociation that depends on the number of monomers in the adsorbed particle is proposed to explain our results. The predictions from this model are solved semianalytically and they are validated using two different surfaces.

To accurately quantify protein adsorption and desorption on PEG-coated surfaces, we imaged individual fluorescently labeled BSA by total internal reflection fluorescence (TIRF) microscopy [13]. Proteins were diluted to low concentrations (5 nM) in imaging buffer to enable single-molecule detection as they adsorb to and desorb from the solid-liquid interface. The protein solution was allowed to equilibrate for at least 1 hour and then the solution was injected into a flow cell that has been constructed with one surface consisting of a coverslip functionalized with PEG brushes. The flow cell does not let water evaporate, so that protein concentration in solution is constant for the duration of the experiment. Immediately following injection of the solution, microscopy videos were collected for 100 min (5000 frames). The inset in Fig. 1(a) shows a representative adsorbed BSA image. Individual fluorophores are clearly visible above the fluorescence background making it easy to detect the moment of adsorption and desorption from the surface.

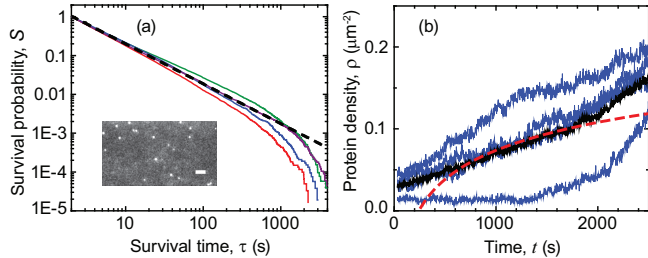


FIG. 1. Anomalous surface kinetics. (a) The survival probability of BSA molecules on PEG surface does not exhibit an exponential decay. Instead it appears to decay as a power law. Four different surfaces are shown (solid lines) together with a power law ( $\tau^{-\alpha}$ , dashed line). Inset: fluorescent image of adsorbed BSA. Scale bar is  $3 \mu\text{m}$ . (b) The protein surface density increases over time. Here, the  $x$ -axis represents the time since the protein solution is introduced into the flow cell. Four experimental surfaces are shown (thin blue lines), together with the density average (black line) and the fit to Eq. (4) as a dashed red line.

Our single-molecule assay allows an evaluation of the kinetic model because both  $k_{\text{ads}}$  and  $k_{\text{des}}$  can be directly measured. In particular, Eq. (1) predicts an average dwell time for an adsorbed particle on the surface to be  $\langle \tau \rangle = 1/k_{\text{des}}$  and the dwell times themselves to be a random variable drawn from an exponential distribution

$\psi(\tau) = k_{\text{des}} \exp(-k_{\text{des}}\tau)$ . Fig. 1(a) shows the survival probabilities,  $S(\tau)$  of BSA molecules on four independent PEG surfaces,

$$S(\tau) = \int_{\tau}^{\infty} \psi(t) dt. \quad (2)$$

Contrary to the expectations from the simple kinetic model (Eq. (1)), the survival probability  $S(\tau)$  does not decay exponentially. Counterintuitively, it decays as a power law up to a timescale of the order of 1000 s. The surface density is observed to scale as  $S(\tau) \sim S_0 \tau^{-\alpha}$  with  $\alpha = 0.95$ . After 1000 s, the survival probability decays rapidly (exponentially) due to photobleaching. Indeed, when we increase the frame rate from  $0.5 \text{ s}^{-1}$ , to  $10 \text{ s}^{-1}$  (with the same exposure time of 90 ms/frame), the photobleaching decay is observed to occur much earlier (Supplemental Figure S1 [13]).

The observed anomalous desorption kinetics implies that Eq. (1) does not hold and the protein surface density should not reach a steady state within this long timescale, but it should instead increase with time. The surface dwell time (i.e., the desorption time) is given by Eq. (2) as  $\psi(\tau) \sim \alpha S_0 \tau^{-(1+\alpha)}$ . Thus, we can write a recurrence relation for the occupation probability  $P_{\text{on}}$  of an individual surface site,

$$\frac{dP_{\text{on}}(t)}{dt} = A_1 k_{\text{ads}} P_{\text{off}}(t) - \int_0^t A_1 k_{\text{ads}} P_{\text{off}}(t') \psi(t-t') dt', \quad (3)$$

where  $P_{\text{off}}(t)$  is the probability of the site being empty at time  $t$ , with  $P_{\text{off}}(t) + P_{\text{on}}(t) = 1$ , and  $A_1$  is the area of a single site. The first term in the right part of Eq. (3) has the same meaning as the adsorption in Eq. (1) and the second term accounts for a particle being adsorbed at an earlier time  $t' < t$  and desorbing at time  $t$ . It is possible to solve for  $P_{\text{on}}(t)$  by use of Laplace transform, which yields  $P_{\text{on}}(t) \sim 1 - t^{\alpha-1}/c_1$  [13]. Note that, assuming again low surface occupation, the surface density is proportional to the probability of occupation of a single site and thus

$$\rho(t) \sim \frac{1}{A_1} \left( 1 - \frac{t^{\alpha-1}}{c_1} \right), \quad (4)$$

where  $c_1 = A_1 k_{\text{ads}} S_0 \Gamma(1-\alpha) \Gamma(\alpha)$ . Fig. 1(b) shows the density of surface proteins as a function of time for 3000 s in four replicate experiments. The protein density increases with time without reaching a steady state.

A power-law tail in the dwell times can emerge from two different scenarios [14]: (1) A non-stationary process where after capture, the trap strength becomes stronger with time and the particle probability of escape decreases [15] and (2) a heterogeneous process involving traps of varying depths [16–19]. Here, we were able to untangle these effects by measuring the intensity of adsorbed particles as a function of the time that lapsed since protein adsorption. The key idea behind this measurement lies

in the fact that a protein aggregate will be bound more strongly to the surface while at the same time it will exhibit brighter fluorescence emission. Fig. 2 shows, as a black line, the average fluorescence intensity for all particles as a function of the time they spent on the surface. The average intensity increases with time since adsorption. Then, in red, green, and blue the figure shows the average intensity for those particle that survived on the surface at least 200, 400, and 1000 s, respectively. Interestingly, the particles that survived more time on the surface were brighter since the time of adsorption. This result suggests that molecules form aggregates in solution and then they bind to the surface. Note that, e.g. for particles that survive longer than 1000 s, an increase is also seen up to 1000 s, suggesting that surface-mediated cluster growth can also take place.

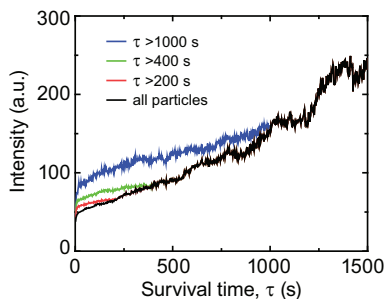


FIG. 2. Average intensities of the fluorescent particles as a function of the time that lapsed since particle adsorption on the surface. The colored lines show the average intensity for particles that dwell on the surface for longer than a given threshold (200, 400, or 1000 s in red, green, and blue, respectively).

The histogram of particle intensities (Fig. 3(a)) displays several well-differentiated peaks, in agreement with our hypothesis that particles with different numbers of BSA proteins are found on the surface, i.e., we observe an intensity peak for single proteins ( $n = 1$ ) and peaks for dimers ( $n = 2$ ), trimers ( $n = 3$ ), etc. Following the same methodology we employed above, we measure the intensity histograms of particles that dwell on the surface for times longer than  $\tau$ . Three different histograms are shown as examples in Fig. 3(a), corresponding to  $\tau = 200, 400$ , and  $1000$  s. While the overall survival probability of adsorbed particles decays as a power law, the survival probability of each of the different peaks decay exponentially, albeit with different characteristic times (Fig. 3(b)).

Given that particles with longer dwell times are brighter and that fluorescent particles on the surface have well-defined discrete intensities, we postulate a simple model where proteins in solution can aggregate into larger clusters. Classical biochemistry usually considers that proteins unfold when they aggregate. However, this process would be irreversible for practical pur-

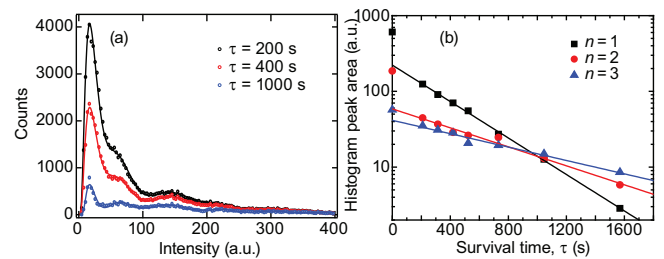
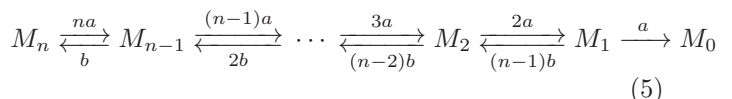


FIG. 3. Particle intensities show discrete peaks. (a) Histograms of detected particle intensities for particles that survive on the surface longer than  $\tau = 200, 400$ , and  $1000$  s. Several peaks are observed in the histograms. (b) Survival of the first three peaks as a function of time, which correspond to single monomer, dimer, and trimer. The survival is shown as peak area for particles that dwell on the surface longer than  $\tau$ , instead of actual probability, to preserve the area ratios between different peaks.

poses and particles would sediment out of the liquid phase. Our solution is in equilibrium and thus we assume particles can reversibly self-associate into soluble multimers [20, 21]. The distribution of number of proteins ( $n$  monomers) in a multimer in equilibrium,  $p(n)$ , should follow a Boltzmann distribution, where the addition of an extra protein requires a free energy  $\Delta F$ . Thus  $p(n) = [\exp(1/n_0) - 1] \exp(-n/n_0)$  with  $n_0$  being the characteristic number of molecules in a particle in solution [13]. Once the particle is on the surface, each constituent monomer has the same probability of association to and dissociation from the surface. Thus, at a given time, any number of monomers between 0 and  $n$  can be associated to the surface,



where  $a$  and  $b$  are the monomer dissociation and association rates,  $M_i$  is a state with  $i$  monomers bound to the surface and  $M_0$  represents a protein that has completely dissociated from the surface. Under the approximation  $a \ll b$ , reaction (5) has the asymptotic long time solution for the probability of being in state  $M_0$

$$p_0(\tau|n) = 1 - \exp(-k_n \tau), \quad (6)$$

where

$$k_n = n \frac{a^n}{b^{n-1}} \quad (7)$$

for any initial condition between the states  $M_1$  and  $M_n$  [13].

The survival probability  $S_n(\tau)$  for a multimer of  $n$  monomers describes the probability that the particle has not yet reached state  $M_0$ . Thus,  $S_n(\tau) = 1 - p_0(\tau|n) = \exp(-k_n \tau)$ . This predicted behavior is in excellent agreement with the exponential decays of the different intensity peaks (Fig. 3(b)). Further, the rate  $k_n$  is observed

to obey the predicted behavior as in Eq. (7) (Fig. 4(a)). This measurement yields  $a/b = 0.34$  and  $b = 0.008 \text{ s}^{-1}$ . Besides allowing the computation of  $k_n$ , an extrapolation of the intensity peaks to  $\tau = 0$  yields the fraction of molecules in each state, i.e., the fraction of single monomers  $p(n=1)$ , dimers  $p(n=2)$ , trimers  $p(n=3)$ , etc., that bind to the surface. Fig. 4b shows that these fractions are in good agreement with our assumption of a Boltzmann distribution for the number of monomers within a particle in solution, where the characteristic number of monomers is found from these data to be  $n_0 = 0.97$ .

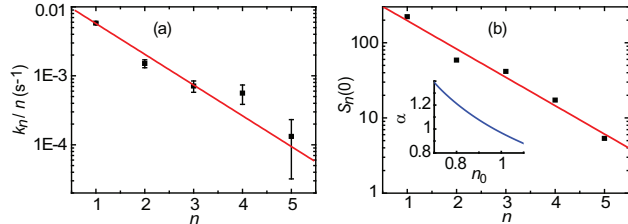


FIG. 4. Desorption characterization of particles with different number of monomers. (a) The desorption rate for particles with  $n$  monomers is predicted to be  $k_n = nb(a/b)^n$ . Thus the ratio  $k_n/n$  is shown as a function of  $n$  to corroborate this prediction. (b) Peak area under each peak extrapolated to  $\tau = 0$ . This value represents the relative amount of adsorbed particles found for each number of monomers. Inset: anomalous exponent  $\alpha$  according to Eq. (9) when  $a/b$  is set to 0.34.

How does a power-law tail in the surface dwell time distribution emerge? Even though the dwell times of particle of a given number of monomers are exponentially distributed, the asymptotic dwell times of a particle of unknown  $n$  can have a power-law form. Namely, the survival probability is

$$S(\tau) = \sum_{n=1}^{\infty} S_n(\tau)p(n) \quad (8)$$

$$\sim \sum_{n=1}^{\infty} \exp \left[ -nb \left( \frac{a}{b} \right)^n \tau - \frac{n}{n_0} \right].$$

We analyzed this function numerically and found that, at long times, it converges to a power-law tail (Supplemental Fig. S2) for a wide range of  $a$ ,  $b$ , and  $n_0$  parameters. A systematic numerical analysis of Eq. (8) reveals  $S(\tau) \sim \tau^{-\alpha}$  with

$$\alpha = \frac{\gamma}{n_0} f \left( \frac{a}{b} \right), \quad (9)$$

where  $\gamma$  is a constant and  $f(x)$  is a monotonically increasing function (Supplemental Fig. S3). Note that  $\alpha$  only depends on the dissociation/association rates ( $a$  and  $b$ ) via their ratio. By setting  $a/b = 0.34$  as found from Fig. 4(a), we obtain the dependence of  $\alpha$  on the characteristic number of monomers in a particle,  $n_0$  (inset

of Fig. 4(b)). An anomalous exponent  $\alpha = 0.95$  (as obtained for the tail of the survival probability) is found for  $n_0 = 1.0$ . This value is in surprisingly good agreement with the average value from the relative magnitude of the intensity peaks (Fig. 4(b)).

Only two parameters are responsible for the anomalous kinetics behavior: the tendency of the proteins in solution to polymerize, characterized by the characteristic number of monomers in a single particle, and the ratio between adsorption and desorption rates of a single monomer within a particle on the surface. In order to evaluate our findings on a different set of parameters, we modified the PEG conditions to yield a different adsorption/desorption ratio. Specifically, we prepared a new PEG brush surface with a higher grafting density [13]. While the original PEG surface had an average grafting density of  $0.15 \pm 0.03$  chains/ $\text{nm}^2$ , the modified surface had an average density of  $0.31 \pm 0.03$  chains/ $\text{nm}^2$ , as measured by ellipsometry. The multimer model was also found to be in good agreement with the measured kinetics in this surface. A multimodal population was detected in the histogram of particle fluorescent intensity and each peak decayed exponentially with time (Fig. 5(a)). The rate of release from the surface was also observed to obey the behavior predicted by Eq. (7) (Fig. 5(b)) and the survival probability exhibits power-law behavior (Supplemental Fig. S4). However, in this case the ratio between monomer binding and unbinding was different than previously found for the low density PEG surface. In this case we obtained  $a/b = 0.57$ , which does not allow us to use the small  $a/b$  approximation. Thus, a model without this approximation should be evaluated in this case [13].

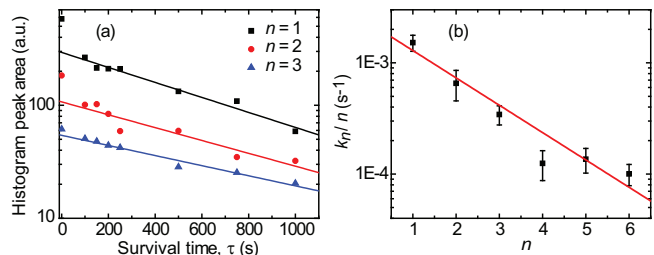


FIG. 5. Desorption characterization of particles from a high-density PEG surface. (a) Survival of the first three peaks, i.e. peak area for particles that dwell on the surface longer than a time  $\tau$  as a function of the time  $\tau$ . (b) Desorption rate from high density PEG for particles with  $n$  monomers. The ratio  $k_n/n$  is shown as a function of  $n$  in the same manner as shown in Fig. 4(a).

In order to analyze the adsorption and desorption kinetics on low-fouling surfaces, we studied the kinetics of BSA on PEG-coated silica surfaces. Our experimental data show that the release from the surface is not governed by an intuitive constant release rate and as a consequence, the distribution of dwell times on the surface is

not exponential. Conversely, the dwell times are drawn from a power-law distribution. This anomalous kinetics is found to be rooted in multimers being reversibly formed in solution, where each multimer has a release rate that depends on the number of monomers.

**Acknowledgement.** We thank Xinran Xu for technical assistance with imaging. This work was supported by the National Science Foundation (award number 1511830).

- 
- \* Corresponding authors: mkipper@colostate.edu, diego.krapf@colostate.edu
- [1] J J Ramsden, “Puzzles and paradoxes in protein adsorption,” *Chem. Soc. Rev.* **24**, 73–78 (1995).
- [2] Jeffrey J Gray, “The interaction of proteins with solid surfaces,” *Curr. Opin. Struct. Biol.* **14**, 110–115 (2004).
- [3] Michael Rabe, Dorinel Verdes, and Stefan Seeger, “Understanding protein adsorption phenomena at solid surfaces,” *Adv. Colloid Interface Sci.* **162**, 87–106 (2011).
- [4] Zbigniew Adamczyk, “Modeling adsorption of colloids and proteins,” *Curr. Opin. Colloid Interface Sci.* **17**, 173–186 (2012).
- [5] Qiang Wei, Tobias Becherer, Stefano Angioletti-Uberti, Joachim Dzubiella, Christian Wischke, Axel T Neffe, Andreas Lendlein, Matthias Ballauff, and Rainer Haag, “Protein interactions with polymer coatings and biomaterials,” *Angew. Chem. Int. Ed. Engl.* **53**, 8004–8031 (2014).
- [6] Robert A Latour, “Biomaterials: protein–surface interactions,” in *Encyclopedia of Biomaterials and Biomedical Engineering*, Vol. 1, edited by G L Bowlin and G Wnek (CRC Press, 2005) pp. 270–284.
- [7] Fang Fang, Javier Satulovsky, and Igal Szleifer, “Kinetics of protein adsorption and desorption on surfaces with grafted polymers,” *Biophys. J.* **89**, 1516–1533 (2005).
- [8] Mohommadhasan Hedayati, Megan J Neufeld, Melissa M Reynolds, and Matt J Kipper, “The quest for blood-compatible materials: Recent advances and future technologies,” *Mater. Sci. Eng. R Rep.* **138**, 118–152 (2019).
- [9] Mohammadhasan Hedayati, Melissa M Reynolds, Diego Krapf, and Matt J Kipper, “Nanostructured surfaces that mimic the vascular endothelial glycocalyx reduce blood protein adsorption and prevent fibrin network formation,” *ACS Appl. Mater. Interfaces* **10**, 31892–31902 (2018).
- [10] Rahul Roy, Sungchul Hohng, and Taekjip Ha, “A practical guide to single-molecule FRET,” *Nature methods* **5**, 507 (2008).
- [11] Indrani Banerjee, Ravindra C Pangule, and Ravi S Kane, “Antifouling coatings: recent developments in the design of surfaces that prevent fouling by proteins, bacteria, and marine organisms,” *Adv. Mater.* **23**, 690–718 (2011).
- [12] Hyeran Noh and Erwin A Vogler, “Volumetric interpretation of protein adsorption: competition from mixtures and the Vroman effect,” *Biomaterials* **28**, 405–422 (2007).
- [13] See Supplemental Material at [URL will be inserted by publisher] for materials and methods, mathematical derivations, and supplemental figures.
- [14] Diego Krapf, “Mechanisms underlying anomalous diffusion in the plasma membrane,” in *Curr. Top. Membr.*, Vol. 75 (Elsevier, 2015) pp. 167–207.
- [15] Aubrey V Weigel, Michael M Tamkun, and Diego Krapf, “Quantifying the dynamic interactions between a clathrin-coated pit and cargo molecules,” *Proc. Natl. Acad. Sci. U.S.A.* **110**, E4591–E4600 (2013).
- [16] Harvey Scher and Elliott W Montroll, “Anomalous transit-time dispersion in amorphous solids,” *Phys. Rev. B* **12**, 2455 (1975).
- [17] IM Sokolov, SB Yuste, JJ Ruiz-Lorenzo, and Katja Lindenberg, “Mean field model of coagulation and annihilation reactions in a medium of quenched traps: Subdiffusion,” *Phys. Rev. E* **79**, 051113 (2009).
- [18] Stas Burov, Jae-Hyung Jeon, Ralf Metzler, and Eli Barkai, “Single particle tracking in systems showing anomalous diffusion: the role of weak ergodicity breaking,” *Phys. Chem. Chem. Phys.* **13**, 1800–1812 (2011).
- [19] Diego Krapf, “Nonergodicity in nanoscale electrodes,” *Phys. Chem. Chem. Phys.* **15**, 459–465 (2013).
- [20] Mary EM Cromwell, Eric Hilario, and Fred Jacobson, “Protein aggregation and bioprocessing,” *AAPS J.* **8**, E572–E579 (2006).
- [21] Harold P Erickson, “Basic thermodynamics of reversible association,” in *Principles of Protein-Protein Association* (IOP Publishing, 2019) pp. 2–1 to 2–7.

# Supplemental Material for “Anomalous protein adsorption/desorption kinetics on low-fouling surfaces”

Mohammadhasan Hedayati,<sup>1</sup> Matt J. Kipper,<sup>1,2,3</sup> and Diego Krapf<sup>2,3,4</sup>

<sup>1</sup>*Department of Chemical and Biological Engineering,  
Colorado State University, Fort Collins, CO 80523, USA*

<sup>2</sup>*School of Biomedical Engineering, Colorado State University, Fort Collins, CO 80523, USA*

<sup>3</sup>*School of Advanced Materials Discovery, Colorado State University, Fort Collins, CO 80523, USA*

<sup>4</sup>*Department of Electrical and Computer Engineering,  
Colorado State University, Fort Collins, CO 80523, USA*

## MATERIALS AND METHODS

### Materials

PEG silane (2-[methoxy(polyethyleneoxy)6-9propyl]trimethoxysilane), MW 459–591 Da, was purchased from Gelest (Morrisville, PA).  $\beta$ -Mercaptoethanol, catalase from bovine liver, and glucose oxidase were purchased from Sigma Aldrich (St. Louis, MO). Anhydrous toluene was purchased from MilliporeSigma (Burlington, MA). BSA conjugated to Alexa Fluor 647 and ethanol (200 proof 99.5+%) was purchased from Thermo Fisher Scientific (Waltham, MA). 18.2 M $\Omega$  cm water from a Millipore water purification unit was used for making all aqueous solutions.

### Preparation of PEG brush surfaces

Surfaces functionalized with PEG brushes were constructed via a grafting-to approach [1, 2]. Prior to functionalization, fused silica wafers were thoroughly washed with acetone, ethanol, and deionized water and dried with ultrapure N<sub>2</sub>. Wafers were then exposed to oxygen plasma under vacuum for 10 min. The substrates were subsequently incubated in 1% v/v PEG silane dissolved in anhydrous toluene. The reaction was performed at room temperature for 20 min to construct PEG brush surfaces. Finally, surfaces were rinsed multiple times with toluene and deionized water and dried with ultrapure N<sub>2</sub>. The higher grafting density surfaces were made by incubating the PEG solution for 1 hour instead of 20 min.

### PEG characterization

The thickness of the dry brush was measured by ellipsometry. For this purpose PEG brushes were constructed on Si wafers using the same protocol described above.  $\langle 100 \rangle$  p-doped 10-20  $\Omega$ -cm Si wafers were purchased from MSE Supplies (Tucson, AZ). Ellipsometry was performed using a J.A. Woollam variable angle spectroscopic ellipsometer (model VASE-VB-250) and data analysis was done using the J. A. Woollam WVASE32 software package. Each surface was spectrally scanned with an incident angle between 60 – 80°, in increments of 5°, over a wavelength range of 500 – 900 nm. The collected spectra were fit to a three-layer planar model of the solid surface, which accounts for the refractive index of air ( $n = 1.003$ ), PEG ( $n = 1.430$ ), silicon oxide layer ( $n = 1.457$ ), and silicon ( $n = 3.881$ ). The dry PEG brush thickness  $h$  was obtained and subsequently related to grafting density  $\sigma_{\text{PEG}} = \rho_{\text{dry}} h N_A / M_w$  where  $\rho_{\text{dry}}$  is the dry density of the PEG monomer repeat unit (1 g/cm<sup>3</sup>),  $N_A$  is Avogadro’s number, and  $M_w$  is the average molecular weight of the PEG polymer (500 Da). For each surface preparation, dry thickness was measured on three different samples and on two different spots in each sample. The resulting grafting density was  $0.15 \pm 0.03$  nm<sup>-2</sup>. The density of the high grafting density PEG was found to be  $0.31 \pm 0.03$  nm<sup>-2</sup>.

### Imaging buffer

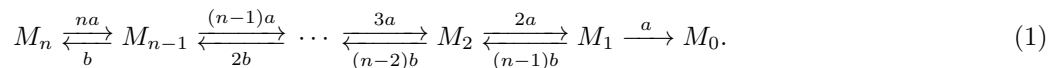
For imaging purposes BSA was diluted in a buffer consisting of 50 mM Tris-HCl (pH 8.0), 10 mM NaCl, 0.8% glucose, 0.15 mg mL<sup>-1</sup> glucose oxidase, 34  $\mu$ g mL<sup>-1</sup> catalase, and 1%  $\beta$ -mercaptoethanol. This buffer includes an enzymatic oxygen scavenging system and  $\beta$ -mercaptoethanol to increase fluorophore stability [3].

## Imaging

Images were acquired by time-lapse imaging using Nikon NIS-Elements 4.51 software in an an objective-type total internal reflection fluorescence (TIRF) custom-built microscope equipped with an Olympus PlanApo 100× NA1.45 objective and a CRISP ASI autofocus system [4]. The optical aberrations of the imaging system were corrected using a MicAO 3DSR adaptive optics system (Imagine Optic, Orsay, France) inserted into the emission pathway between the microscope and the EMCCD camera [5]. Fluorophores were excited with a 638-nm laser (DL638-328 050, CrystaLaser, Reno, NV) under continuous illumination. For excitation, an optical density filter with ND=1.5 was used and an incident angle below the critical angle was chosen to provide a penetration depth of multiple micrometers. Emission was collected through the appropriate Semrock bandpass filters and the images were acquired in a water-cooled, back-illuminated EMCCD camera (iXon DU-888, Andor, Belfast, UK) liquid-cooled to  $-85^\circ\text{C}$  with an electronic gain of 60 at a rate of 0.5 frames/s over a total period of 10000 frames. Exposure time was limited to 90 ms to avoid photobleaching.

### MULTIMERIC DESORPTION MODEL

The desorption reaction for a multimer of  $n$  monomers can be written as



To provide an example of how we solve the temporal evolution of this reaction we employ the case  $n = 3$ . In this case, the reaction simplifies to



Casting this reaction into a set of differential equations yields

$$\begin{aligned} \frac{dp_3}{dt} &= -3a p_3 + b p_2 \\ \frac{dp_2}{dt} &= 3a p_3 - (2a + b) p_2 + 2b p_1 \\ \frac{dp_1}{dt} &= 2a p_2 - (a + 2b) p_1 \\ \frac{dp_0}{dt} &= a p_1. \end{aligned}$$

Considering that when a molecule adsorbs to the surface it should bind via one of its monomers, the initial condition is setting the system in state  $M_1$ . However, the long-time evolution of the system is not sensitive to its initial condition (as long as it is not in state  $M_0$ ). Thus we set  $p_1(0) = 1$  and  $p_0(0) = p_2(0) = p_3(0) = 0$ . In order to solve the set of differential equations we employ a Laplace transform,

$$\begin{aligned} s p_3(s) &= -3a p_3(s) + b p_2(s) \\ s p_2(s) &= 3a p_3(s) - (2a + b) p_2(s) + 2b p_1(s) \\ s p_1(s) - 1 &= 2a p_2(s) - (a + 2b) p_1(s) \\ s p_0(s) &= a p_1(s). \end{aligned}$$

which is solved to yield

$$p_0(s) = \frac{a [6a^2 + (5a + b)s + s^2]}{s [6a^3 + (11a^2 + 7ab + 2b^2)s + (6a + 3b)s^2 + s^3]}. \quad (3)$$

To solve for the long time asymptote, we consider the small  $s$  behavior,

$$p_0(s) = \frac{6a^3}{s [6a^3 + (11a^2 + 7ab + 2b^2)s]}. \quad (4)$$

The inverse Laplace transform of  $p_0(s)$  is

$$p_0(t) = 1 - \exp(-k_3 t), \quad (5)$$

where

$$k_3 = \frac{6a^3}{11a^2 + 7ab + 2b^2}. \quad (6)$$

Further, when the adsorption is faster than desorption as should be the case for a particle on the surface, we have  $a \ll b$  and we can rewrite Eq. (6) as

$$k_3 = 3\frac{a^3}{b^2}. \quad (7)$$

Following the same methodology, it is shown for any chosen  $n$ , in the limit  $a \ll b$ , that

$$k_n = n\frac{a^n}{b^{n-1}}. \quad (8)$$

### DISTRIBUTION OF MULTIMER SIZES

Individual proteins in solution can spontaneously overcome a free energy barrier to dimerize. Subsequently, this soluble dimer can dissociate into single monomers or spontaneously associate to another monomer to form a soluble trimer, and so on. The overall reaction can be described as



Assuming that each additional monomer requires a free energy  $\Delta F$ , the overall energy of a multimer of size  $n$  is  $n\Delta F$ . In thermodynamic equilibrium the system obeys a Boltzmann distribution,

$$p(n) = c \exp(-n\Delta F/k_B T) \quad (10)$$

where  $k_B T$  is thermal energy and  $c$  is a normalization constant. The characteristic number of monomers is  $n_0 = k_B T \Delta F$  and the normalization constant is  $c = \exp(1/n_0) - 1$ .

### SURFACE COVERAGE

As discussed in the main text, the probability that a site is occupied obeys the recurrence relation

$$\frac{dP_{\text{on}}(t)}{dt} = kP_{\text{off}}(t) - \int_0^t kP_{\text{off}}(t')\psi(t-t')dt', \quad (11)$$

where  $P_{\text{on}}(t)$  is the probability of the site being occupied and  $P_{\text{off}}(t)$  is the probability of the site being empty at time  $t$ ,

$$P_{\text{off}}(t) + P_{\text{on}}(t) = 1, \quad (12)$$

and for notation simplicity we have used  $k = k_{\text{ads}}A_1$ , where  $k_{\text{ads}}$  is the adsorption rate with units of  $\mu\text{m}^{-2}\text{s}^{-1}$  and  $A_1$  is the area of a single site. Because  $\frac{dP_{\text{on}}(t)}{dt} = -\frac{dP_{\text{off}}(t)}{dt}$ , we can rewrite Eq. (11) as

$$\frac{dP_{\text{off}}(t)}{dt} = -k \left[ P_{\text{off}}(t) - \int_0^t P_{\text{off}}(t')\psi(t-t')dt' \right]. \quad (13)$$

The second term on the right has the form of a convolution and can thus be solved using a Laplace transform,

$$sP_{\text{off}}(s) - 1 = -k [P_{\text{off}}(s) - P_{\text{off}}(s)\psi(s)], \quad (14)$$

where we have assumed the site is empty at  $t = 0$ , i.e.  $P_{\text{off}}(t = 0) = 1$ . We can obtain the Laplace transform of  $\psi(t)$  by using the Tauberian theorem on the survival probability [6]. Namely, given  $S(t) \sim S_0/t^\alpha$  we obtain

$$S(s) = S_0\Gamma(1 - \alpha)s^{\alpha-1} \quad (15)$$

in the small  $s$  limit. Then we can find  $\psi(s)$  from the relation

$$S(t) = 1 - \int_t^\infty \psi(t')dt' \quad (16)$$

that yields  $\psi(s) = 1 - sS(s)$ . Thus

$$\psi(s) = 1 - S_0\Gamma(1 - \alpha)s^\alpha. \quad (17)$$

Combining Eq. (17) and Eq. (14), we can solve for  $P_{\text{off}}(s)$ :

$$P_{\text{off}}(s) = \frac{1}{s + kS_0\Gamma(1 - \alpha)s^\alpha} \quad (18)$$

and in the limit  $s \rightarrow 0$ , it is further simplified into

$$P_{\text{off}}(s) = \frac{1}{kS_0\Gamma(1 - \alpha)s^\alpha} \quad (19)$$

when  $\alpha < 1$ . Again using the Tauberian theorem, we can invert  $P_{\text{off}}(s)$ :

$$P_{\text{off}}(t) \sim \frac{t^{\alpha-1}}{kS_0\Gamma(1 - \alpha)\Gamma(\alpha)}. \quad (20)$$

By using Eq. (12), we can find the time dependence of  $P_{\text{on}}$ ,

$$P_{\text{on}}(t) \sim 1 - \frac{t^{\alpha-1}}{kS_0\Gamma(1 - \alpha)\Gamma(\alpha)}. \quad (21)$$

At last, the surface density is

$$\rho(t) = \frac{P_{\text{on}}(t)}{A_1}. \quad (22)$$

### MULTIMERIC DESORPTION WHEN $a/b \ll 1$

When  $a/b \ll 1$ , we cannot neglect higher order terms in  $a/b$  that lead to Eq. (7) and Eq. (8). Without these approximation, we were unable to obtain a full expression for any number of monomers  $n$ . Here, we solve for the first six terms in  $S(\tau) = \sum_n S_n(\tau)p(n)$ , where  $S_n(\tau) = \exp(-k_n\tau)$ , and  $p(n)$  follows a Boltzmann distribution (Eq. (10)).

Solving the multimer desorption reaction (Eq. (1)) for  $1 \leq n \leq 5$  yields

$$\begin{aligned} k_1 &= a \\ k_2 &= \frac{2a^2}{b + 3a} \\ k_3 &= \frac{3! a^3}{2b^2 + 7ab + 11a^2} \\ k_4 &= \frac{4! a^4}{3! b^3 + 26ab^2 + 46a^2b + 50a^3} \\ k_5 &= \frac{5! a^5}{4! b^4 + 126ab^3 + 274a^2b^2 + 326a^3b + 274a^4} \end{aligned}$$

Given these five terms, the survival probability  $S(\tau)$  using  $a/b = 0.57$  as found for the high density PEG is shown in Fig. S5.

- 
- [1] Leonid Ionov, Alla Synytska, Elisabeth Kaul, and Stefan Diez, “Protein-resistant polymer coatings based on surface-adsorbed poly (aminoethyl methacrylate)/poly (ethylene glycol) copolymers,” *Biomacromolecules* **11**, 233–237 (2009).
  - [2] David Faulón Marruecos, Mark Kastantin, Daniel K Schwartz, and Joel L Kaar, “Dense poly (ethylene glycol) brushes reduce adsorption and stabilize the unfolded conformation of fibronectin,” *Biomacromolecules* **17**, 1017–1025 (2016).
  - [3] Rahul Roy, Sungchul Hohng, and Taekjip Ha, “A practical guide to single-molecule FRET,” *Nature methods* **5**, 507 (2008).
  - [4] Grace Campagnola, Kanti Nepal, Bryce W Schroder, Olve B Peersen, and Diego Krapf, “Superdiffusive motion of membrane-targeting C2 domains,” *Sci. Rep.* **5**, 17721 (2015).
  - [5] María G Gervasi, Xinran Xu, Blanca Carbajal-Gonzalez, Mariano G Buffone, Pablo E Visconti, and Diego Krapf, “The actin cytoskeleton of the mouse sperm flagellum is organized in a helical structure,” *J. Cell Sci.* **131**, jcs215897 (2018).
  - [6] Joseph Klafter and Igor M Sokolov, *First steps in random walks: from tools to applications* (Oxford University Press, 2011).

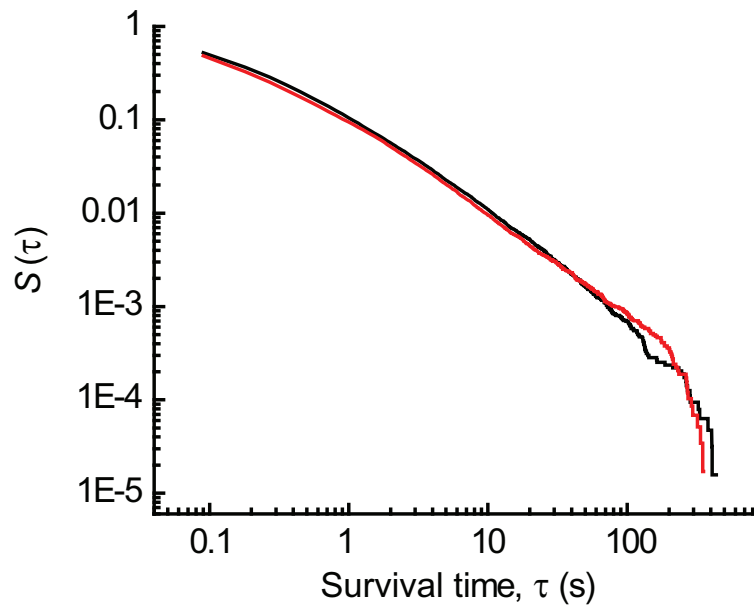


FIG. S1. The survival probability of BSA molecules on PEG surface. The data is similar to that of Fig. 1a in the main text, but the frame rate is 10 fold higher, while the exposure time within each frame is the same. As a consequence, the decay due to photobleaching takes place 10 times faster.

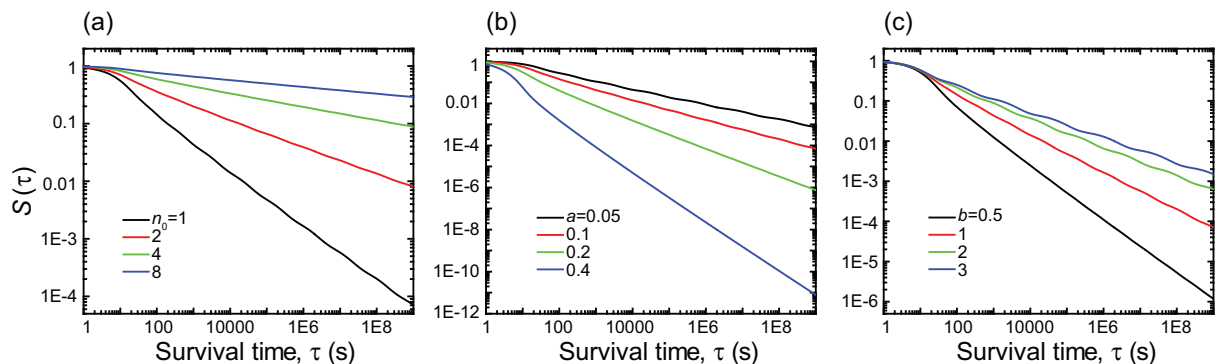


FIG. S2. Survival probability  $S(\tau)$  according to the multimer model presented in the main text exhibits a power law tail. The dwell time of particles on the surface obeys an exponential distribution,  $S_n(\tau) = \exp(-k_n\tau)$ , with mean time,  $1/k_n$  that depends on the number of monomers within the adsorbed particle. The *a priori* probability is given by  $S(\tau) = \sum_{n=1}^{\infty} S_n(\tau)p(n)$  where  $p(n)$  is the probability of the particle having  $n$  monomers and it obeys a Boltzmann distribution with characteristic number of monomers  $n_0$ . (a) Survival probability for different  $n_0$  values. Note that larger  $n_0$  means higher probability of the proteins to self-associate. Binding coefficient is  $b = 1$  and unbinding rate is  $a = 0.1$ . (b) Survival probability for different surface dissociation coefficients  $a$ . Binding coefficient is  $b = 1$  and characteristic number of monomers is  $n_0 = 1$ . (c) Survival probability for different surface binding affinities  $b$ . Dissociation coefficient is  $a = 0.1$  and characteristic number of monomers is  $n_0 = 1$ . Note that when the ratio  $a/b$  is very low, the survival probability also exhibits oscillations because the different modes separate in time.

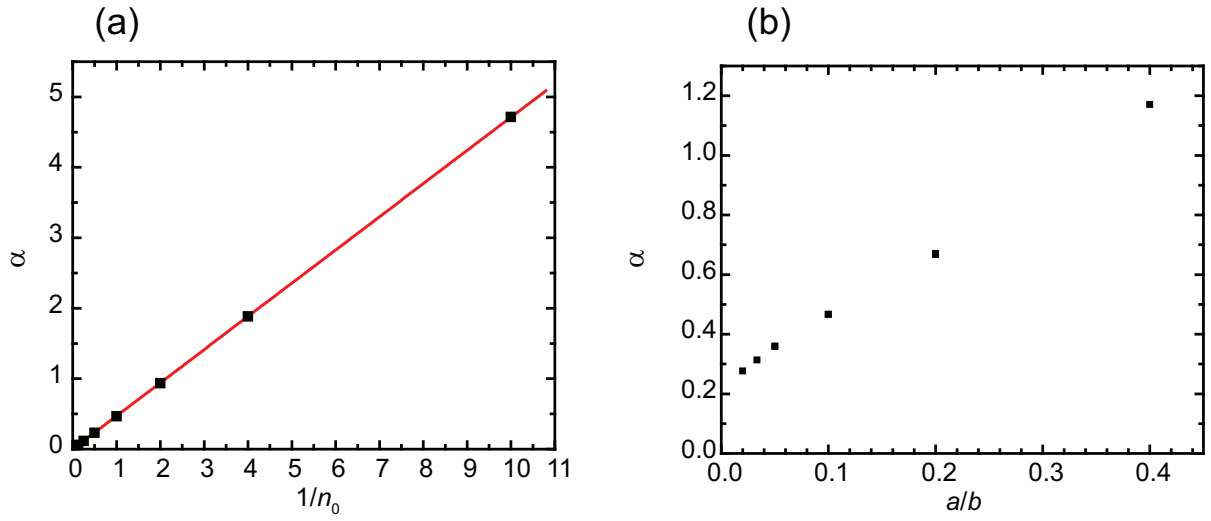


FIG. S3. Anomalous exponent  $\alpha$  in the multimer model, where  $S(\tau) = \sum_{n=1}^{\infty} S_n(\tau)p(n)$  and  $S(\tau) \sim \tau^{-\alpha}$ . The exponent  $\alpha$  is shown for different choices of parameters  $n_0$  (characteristic number of monomers in adsorbed particle) and  $a$  and  $b$  (dissociation and association coefficients, respectively). (a)  $\alpha$  is shown as a function of  $1/n_0$  to highlight the behavior  $S \sim 1/n_0$ . (b)  $\alpha$  is shown as a function of  $a/b$ . Different sets of  $a$  and  $b$  values are used but they all fall within a master curve that only depends on  $a$  and  $b$  via their ratio  $a/b$ .

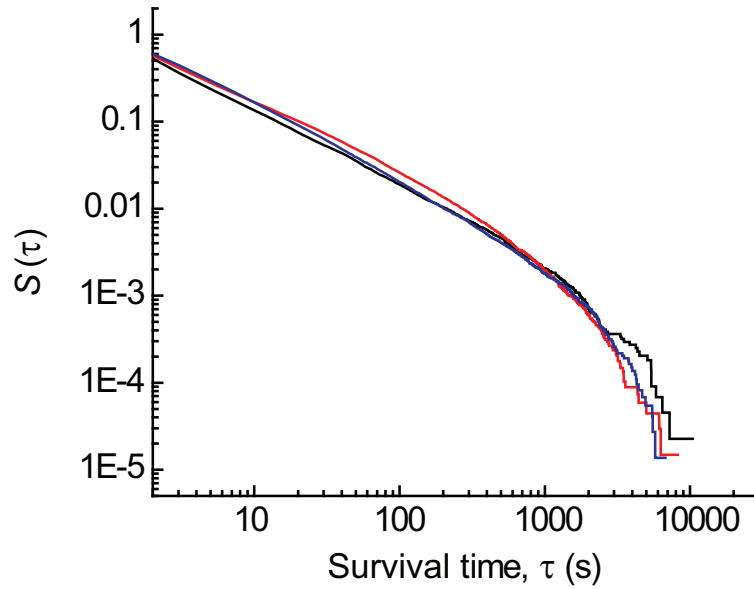


FIG. S4. The survival probability of BSA molecules on high density PEG surface.

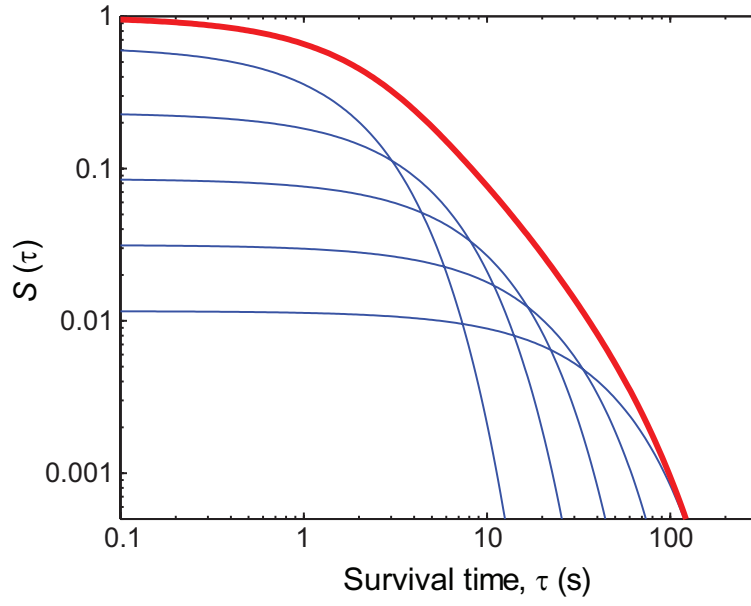


FIG. S5. Survival probability  $S(\tau)$  according to the multimer model when the approximation  $a/b \ll 1$  does not hold. Here,  $a/b = 0.57$ . Namely,  $n_0 = 1$ ,  $a = 0.57$ , and  $b = 1$ . Only the first five modes of  $k_n$  are used. The thin blue lines show the contribution of each of these modes to the survival probability:  $p(n) \exp(-k_n \tau)$ . The thick red line shows the survival probability:  $S(\tau) = \sum_{n=1}^5 S_n(\tau) p(n)$ . This survival probability also shows a power law tail.